Bio-mimetic synthesis of catalytically active nano-silver using *Bos taurus* (A-2) urine

Prashant D Sarvalkar
Shivaji University

Rutuja R Mandavkar
Shivaji University

Mansingraj S Nimbalkar
Shivaji University

Kiran K Sharma
Shivaji University

Pramod S Patil
Shivaji University

Neeraj R Prasad (✉ neeraj_prasad21@rediffmail.com)
Shivaji University

Ganesh S Kamble
KIT, Kolhapur

Abstract

Bio-molecules present in liquid metabolic waste of an Indian cow are effectively used to reduce silver (Ag) ions into Ag nanoparticles (Ag NPs) in one step. This bio-inspired electron transfer to Ag ion for the formation of base Ag metal is fairly prompt and facile. These nanoparticles act as a positive catalyst for various organic transformation reactions. The X-RD pattern of the synthesized product confirmed the formation of Ag nanoparticles. The bio-mimetic Ag NPs show potential activity for degradation of dyes under study. Herein, we have successfully carried out several reduction reactions of nitro groups using Ag nanoparticles as a heterogeneous nanocatalyst.

1. Introduction

Since the dawn of civilization on the planet, material scientists are actively involved in fabrication new materials with desired novel properties. It was observed that the properties of material vary in mixture state as compared with their pure forms e.g. various alloys such as stainless steel, gun metal, wood metal, rose metal, bronze and several composite materials such as re-in forced cement concrete, ply-woods ceramic materials like glass, cements etc bears different properties from the pure constituent parts[1]. Also various type of physical treatment can affect the properties of the materials such as earthen pot after heating beyond a particular temperature becomes porous and does not get dissolved in water. Therefore, earlier attempts have been made to inculcate new properties by mixing two or more materials together in different proportions[2]. Thus the use of innovative material is the mirror of developmental scenario of human civilization and therefore particular age is many times named after the materials in use such as iron age, plastic age and now stepped into nano age[3,4]. Now the scientists working in the domain of material science are mainly interested to develop materials at the nano-scale[5–14]. Due to alien properties nanoparticles find wide range of applications in diverse areas such as in fabrication of various types of sensing devices such as gas sensors, bio-sensors such as blood glucose sensors, oximeter [15], memristors[16], meta-materials[17] which have negative refractive indexes, energy storage devices such as supercapacitors using transition metal oxides, bio-active materials such as anti-microbial and anti-neoplastic agents, heterogeneous catalyst for organic transformation and organic synthesis reactions, heterogeneous catalyst for dye degradation reactions and several types of electronic devices etc. The exotic properties developed in materials at nano-scale is due to various factors such as enlarged surface area this significantly increases active sites for reaction, insignificant gravitational force, possible development of quantum effect, sensitive coulomb's force of attraction or repulsion, alive dangling bonds, constructive random molecular motion, remarkable surface tension and secondary bonds like Van der Waal's attraction etc and these properties make nano-materials different from their bulk counterparts[18–22]. The physical and chemical properties of bulk material are supposed to be constant irrespective of size and weight of material under consideration such as the melting point of metal or refractive index of a liquid are having fixed value. These well-defined physical and chemical properties of the bulk materials reveal interesting properties at nano-scale. But due to exceptional difference in properties at nano-scale from that

of its bulk counterparts many scientists believe the nano regime as a separate state of matter. In fact, the properties of bulk material are an average of the properties at the nano regime.

Our research group has successfully synthesized some transition metal and metal oxide nanoparticles such as Cd, CuO and Pd nanoparticles using Indian cow urine. In the current experimentation process, we have successfully synthesized Ag nanoparticles using A-2 type cow urine. *Ayurveda* is an ancient system of natural and holistic medicine developed particularly in Indian sub-continent. *Ayurveda* literature describes the use of cow products for medicinal purposes. Liquid metabolic waste of cow is a constituent of *Panchagavya* (a combination of cow urine, milk, clarified butter, curd and dung). According to description in classical *Ayurvedic* literature, it is useful to control various ailments especially chronic diseases such as seizer disease, skin disease, hepatic diseases, psoriasis, thyroid dis-order, constipation, abdominal diseases, renal disorders, diabetes mellitus, anticonvulsant drug etc. Some medical professionals claims that cow urine effective anti-neoplatic agent[23]. Cow urine is found to have beneficial properties particularly in the area of agriculture and therapeutics. It has been observed that the urine of Indian cow is highly effective and interestingly almost nil or few medical properties are present in urine of crossbred, exotic cows, buffaloes etc. Recent researches showed that cow urine enhances immune status of individual immune status of individual through activating the macrophases and augmenting their engulfment power as well as bactericidal activity.

2. Laboratory Synthesis Of Nanoparticles

The nanoparticles can be categorized as (1) natural nanomaterials, (2) incidental nanomaterials and (3) engineered nanomaterials. Nano-particles possess wonderful exotic properties. Because of continuous requirement of nanoparticles in various appliances researchers intensely synthesized materials of various size and shape and known as engineered nanomaterials. Due to simplicity, comfortable set up, economical consideration and defect free product bottom-up approach is becoming popular and now a day widely adopted. The bottom up route of synthesis implies that the nanostructures are synthesized by stacking atoms onto each other. This gives rise to crystal planes, crystal planes further stack onto one another which results in the formation of nanostructures. Thus bottom up approach can be simply viewed as synthetic route where the building blocks are added to have a nanostructure.[11,18,24–26].

3. Materials And Methods

3.1 Bio-mimetic synthesis of Ag using *Gir* cow urine:

AgNPs were synthesized using the liquid metabolic waste of indigenous Indian healthy *Gir* (A-2) cow of age seven years. The cow was regularly vaccinated by a veterinarian against common livestock diseases like rinderpest and black quarter etc. The cow urine is procured with agreement of animal rearer from cattle farm belonging to village Kaneri, India. The freshly discharged cow urine was collected in a sterile screw-capped bottle and brought in laboratory. The liquid metabolic waste of *Gir* cow was dribbled using filter paper and stored in suitable container at room temperature.

For the experimentation process, analytical grade Ag nitrate precursor was purchased. Here 100 mL of 0.1M $AgNO_3$ solution was prepared by dissolving Ag nitrate in double-distilled water. Then 15 mL 0.1% w/v cetyltrimethylammonium bromide (CTAB) a cationic surfactant was slowly added in above solution with constant stirring. The borosilicate glass made burette was filled with cow urine and drop wise added in Ag nitrate solution with constant stirring. The reaction mixture was maintained in the range of 25–30C temperature. The addition of cow urine results in the formation of dark blackish colored precipitate of Ag in nano form. When 25 mL of cow urine is added there is formation of sufficient amount of precipitate. The colloidal solution was continuously heated till complete evaporation of water content takes place. Then, the black colored solid mass accumulated at the bottom of the beaker was separated using a metallic spatula and then crushed mechanically into fine powder [5,20,21].

3.1 possible reaction mechanism:

The chemical formula for urea is $CO(NH_2)_2$. Here two $-NH_2$ groups are directly attached to carbonyl group i.e. C = O. Actually it looks that urea should be a base due to presence of lone pair of electron on nitrogen atom. But due to electronegative nature of carbonyl group, it becomes a neutral compound. However when urea gets reacted in presence of enzyme urease or at high temperature the following reactions shows the conversion of Urea to Ammonia by hydrolysis.

NH_2-CO-NH_2 ^{Hydrolysis} $NH_3 + H^+ + CNO^-$ [1]

(Urea) (Isocyanate)

$CNO^- + H^+ + H_2O$ $NH_3 + CO_2$ [2]
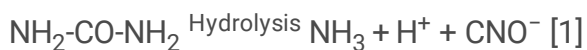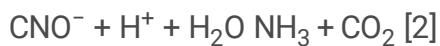
(Ammonia)

In first step of reaction, there is break down of Urea into Ammonia and isocyanate ions as byproduct. This reaction is reversible at pH less than 5 and greater than 12. In second reaction, Isocyanate get hydrolyze to produce Ammonia and carbon dioxide is evolved as a byproduct. Urea hydrolysis is higher at temperature 35^oC than at 15^oC. The effect of pH is only observed between the pH 6 and pH 8.[27]

4. Ramification And Discourse

4.1 Analysis of Synthesized Nanoparticles:

The synthesized nano-particles were characterized using advanced spectroscopic and microscopic techniques. The electron microscopic analysis reveals the morphologies for synthesized nanoparticles.

4.1.1 UV-visible Spectroscopic Examination:

The insoluble black colored power obtained at the end of reaction was sonicated in bath sonicator so as to get well dispersed solution. UV-visible spectroscopic analysis shows maximum absorption is obtained at

500 nm which is in agreement with reported values for AgNPs. The observed increase in absorption value i.e. redshift in λ_{max} value may be due to agglomeration of nanoparticles.

4.1.2 XRD Pattern:

Solid state of materials can be further divided into two types such as crystalline forms and amorphous forms. XRD analysis is applicable to crystalline form of materials only. The XRD pattern reveals formation of poly-dispersed crystalline nano-material. The XRD pattern of biologically synthesized AgNPs is shown in Fig. 2. In XRD pattern, Bragg's reflections are observed at 2θ values of 38.11, 44.19, 64.43, 77.38 and 81.53 representing (111), (200), (220), (311) and (222) planes respectively; which indicates that AgNPs were nanocrystals with cubic face centred (FCC) structure. The peaks in the XRD pattern obtained confirmed that the biosynthesized material was pure AgNPs with highly crystalline nature. The patterns were consistent and are in agreement with the database the Joint Committee on Powder Diffraction Standards (JCPDS) card No. 00-003-0931.

The crystallite size can be calculated famous using Debye−Scherer's formula [28−30].

$$D = \frac{0.9\,\lambda}{\beta \cos\theta}$$

..............(1)

The crystallite size is calculated using above formula and the average size of Ag NPs is 29.92 nm.

Morphology Index (MI)

We are pretty familiar with the ever increasing demand of Ag nanoparticles in various industries. This is because of novel physical, chemical and biological properties developed at nano level. The specific surface area of a nanoparticle depends upon the interrelationship between the particle size and morphology. MI is calculated from FWHM of XRD to explore this relationship, based on report [30].

MI is obtained using the equation,

$$MI = \frac{FWHM_h}{FWHM_h + FWHM_p}$$

...........(2)

Where,

M.I. is morphology index,

$FWHM_h$ is highest FWHM value obtained from peaks.

MI range of experimental Ag NPs ranges from 0.50 to 0.685 and the details are presented in Table.1. It is correlated with the particle size (range from 38.84 to 21.79 nm) and specific surface area (range from

14.71- 26.22 m^2g^{-1}). From the calculated data it is observed that MI is directly proportional to particle size and inversely proportional to specific surface area with a small deviation. The results are shown in Fig.3 & Fig.4. Linear fit in the figures indicates the deviations and relationships between them.

Table No.1 X-RD Analysis and Calculation of Various Parameters

Sr. No.	Peak Position :2θ (degree)	Full width half maxima (A⁰)	Full width half maxima (radians)	Particle Size D(nm)	d-spacing (A⁰)	For Ag unit cell edges: a = b = c (A⁰)	Specific surface area (m²/g)	Morphological indexing
1	38.11	0.2165	0.003778	38.84	2.3592	4.0857	14.71237	0.685
2	44.19	0.3936	0.006869	21.79	2.0481		26.22435	0.545
3	64.43	0.3149	0.005496	29.82	1.4449		19.16259	0.599
4	77.38	0.2755	0.004808	36.95	1.1406		15.46491	0.631
5	81.53	0.4723	0.008243	22.21	1.1796		25.72844	0.500

4.1.3 SEM:

Scanning electron microscopy represents a powerful tool for sample imaging with nanoscale magnification and resolution which visualizes very small topographic details on the surface of object. Synthesis of AgNPs using biological route (either plant extract or animal waste) shows relatively spherical in shape.

Herein Scanning Electron Microscopic (SEM) analysis was done using MIRA3 TESCAN SEM machine. The morphological studies can be determined by Scanning electron microscopy (SEM). Uniformly distributed Ag nanoparticles were observed in SEM. AgNPs were relatively spherical/irregular in shape. The larger Ag nanoparticles may be due to aggregation of the smaller ones. The sample has average diameter nearly 500 nm. The change in size of AgNPs can be seen in Fig. 5.

AgNPs are found to be agglomerated in SEM images. This may be due to addition of excess amount cow urine further presence of impurity remains in synthesized samples may be another cause.

4.1.4 AFM

The Atomic force microscope is the most commonly used form of Scanning probe microscope. Atomic force microscopy is a three dimensional topographic technique with a high atomic resolutions and measures surface roughness. This is very useful to characterize surface defects and to determine the size and conformation of molecules and aggregates on the surface. AFM technique is applicable and effective way to image almost any kind of surfaces. Figure 6 shows the surface topography of Ag thin films observed by AFM in two dimensional and three dimensional views. The image provides at two dimensional

(2D) and three-dimensional (3D) profile of the surface at the nanoscale. The larger Ag nanoparticles may be due to aggregation of the smaller ones. [31,32]

4.1.6 PL spectra

Photoluminescence is the phenomenon of emission of light from any type of matter when photon is incident on it. Photoluminescence (PL) is the tool to confirm the structural defect related properties. Figure 7 shows the PL spectra of Ag nanoparticles. PL spectra is consist of two peaks. First luminescence peaks are at nearly 239 nm which are in UV region, and second peaks are at nearly 314 nm[33,34].

4.1.5 FT-RAMAN

Raman spectroscopy is a powerful tool to analyze structural or morphological properties of solid at a local level given the strong sensitivity of the phonon characteristic to the crystalline nature of the material. Raman spectroscopy is the bulk sensitive technique but use of excitation frequencies allows some surface sensitivity. Figure 8 shows the Raman spectrum of Ag nanoparticles. Curve displays two obvious peaks, corresponding to the D and G bands of Ag nanoparticles. The D and G bands of Ag nanoparticles were respectively observed at 1363 and 1554 cm^{-1}. In addition, we calculated the D/G intensity ratio for the Ag nanoparticles to be ID/IG = 0.94.[35]

4.1.7 FT-IR

FT-IR spectra show absorption bands that enable to determine the presence of various functional groups in a molecule. Various functional groups correspond to different frequencies and hence different wave numbers. A very strong and broad absorption band at 3440 cm^{-1} in Fig. 9 indicates that the synthesized samples can have vibrations of symmetric stretching due to presence of primary amine. The other bands are observed at 1608 and 1124 cm^{-1} which may be due to aromatic stretch of organic compound present in synthesized nanomaterials.

FT-IR spectra are the fingerprint due to presence of functional groups in the material under study. Figure 9 shows FT-IR spectra of *Bos taurus* (A-2 type) cow urine, the observed major peak positions are 3054 cm^{-1} 1617cm^{-1},1362cm^{-1}, which may be due to C-H aromatic stretching, 1617 cm^{-1} C-C aromatic stretching, 1362 cm^{-1} C = O stretching (ketonic group) respectively.

Further Fig. 9 shows peak position at 3440cm^{-1}, 1608cm^{-1}, 1124cm^{-1}. There is red shift in the observed peak position. This may be due to interaction of Ag nanoparticle with function groups viz. C-H and AgNPs interaction, C-C and Ag interaction.

4.1.6 Electro kinetic Potential and Particle Size Distribution:

Electro kinetic potential from Fig. 10 signifies the stability of the synthesized nanoparticles. The hydrodynamic diameter of the synthesized nanoparticles can be discovered using dynamic light scattering. Herein bio-inspired synthesis involves formation of poly-dispersed nanoparticles. The hydrodynamic diameter is measured using Malvern Instruments Ltd. The DLS is represented in Fig. 11 which reveals the hydrodynamic diameter of the synthesized particles.

When the light passed through the colloidal solution, it bombards on small particles and scatters in all possible directions (Rayleigh scattering). We observe a fluctuation in the intensity of light even if the incident light is monochromatic or laser. This fluctuation in intensity of light is due to tiny molecules in solution which continuously undergoes Brownian motion. As a result of the Brownian motion of a particle, the dimension of the particle can be determined. This technique is commonly known as dynamic light scattering and also called as photon correlation scattering

DLS shows mode average particle size was 296.2 nm. The distribution of particles according to size varies from 41.80 to 4737 nm. The particles are made up by biological way thus the particle size of nanoparticles cannot be controlled and it is high in range.

4.1.7 Electro kinetic Potential Analyzer

Electro kinetic potential of the sample reveals the dispersion stability of the colloidal solution. Higher values of electro kinetic potentials predict a more stable dispersion. In fact electro kinetic potential analyzer is an important tool for understanding the state of the surface of the nanoparticle and predicting the long term stability of the nanoparticles. The zeta potential is an indication of the surface potential, and so determines the magnitude of the electric double layer repulsion. Normally, a value 40 to 60 mV indicates good stability of the nanoparticles.

Zeta potential shows the stability of the synthesized nanoparticles. It also shows the mobility of the nanoparticles. Zeta potential analysis of synthesized Ag nanoparticles shows incipient instability i.e -19.02 mV. According to zeta potential results, it was observed that the outer layer of Ag nanoparticles should possess negative charge. The figure shows three cycles reading of the stability and mobility of the nanoparticles. The zeta potential is an indication of the surface potential, and so determines the magnitude of the electrical double layer repulsion. The large positive and large negative value of zeta potential is required for stable dispersion.

5. Ag Nanoparticles As Nano-catalyst:

Reduction process is an important and fundamental of organic transformation in chemical synthesis and industrial chemistry. The description of a catalyst these days can be simply and ideally started with nanoparticles. In the current experimentation process, we have studied several organic transformation reactions using Ag nanoparticles as a heterogeneous nano-catalyst. Here we have tried to convert $-NO_2$ group into $-NH_2$ group using sodium borohydride as reducing agent. Actually sodium borohydride can reduce only the carbonyl group i.e. aldehydic (-CHO) or ketonic (-C⬚O) groups. However, our experimentation reveals that sodium borohydride can successfully reduce $-NO_2$ functional group into $-NH_2$ group in the presence of Ag nanoparticles. The progress of reaction is spectrophotometrically monitored [18,22,24−26,36]. The details of the studied reactions are as below:

5.1.1 Nano-Ag catalyzed conversion of 4-Nitrophenol into 4-Aminophenol:

For the current experimentation process, we purchased analytical grade 4-Nitrophenol ($C_6H_5NO_3$) and Sodium Borohydride ($NaBH_4$), from Sigma Aldrich. About 1 mL ice-cold solution of 0.05M $NaBH_4$ was

taken in the quartz cuvette. Then, in the above solution about 1.5 mL, 0.1 mM 4-Nitrophenol solution was slowly added. To this reaction mixture water suspension of 200 μL (0.1mg/ml) Ag nanoparticles were added.

The absorption peaks responsible for -NO_2 functional group is at wavelength 400 nm which decreases with progress of time whereas a new absorption at 300 nm makes its appearance which is responsible for –NH_2 group. This indicates that complete conversion of 4-Nitrophenol to 4-aminophenol take place within 390 seconds time interval. During this time about 95% of the reactant is converted into product. When we plot a graph of concentration verse time we get a straight line passing through origin. The progress of reaction is shown in Fig. 12.

This is an example of the first-order reaction with a rate constant (k) is 0.3047 min^{-1}.

5.1.2 Nano-Ag catalyzed conversion of 2-Nitroaniline to 2-aminoaniline

Analytical grade 2-Nitroaniline ($C_6H_6N_2O_2$), Sodium Borohydride ($NaBH_4$), were procured from Sigma Aldrich. About 1.5 ml ice-cold solution of 0.05 M $NaBH_4$ was taken in the quartz cuvette. Then, in the above solution, about 1 mL 0.1 mM 2-Nitroaniline solutions were added drop-wise. To this reaction mixture water suspension of 200 μL (0.1mg/ml) Ag nanoparticles were added.

The absorption peak responsible for -NO_2 functional group is at wavelength 413 nm which decreases with progress of time. This indicates that complete conversion of 2-Nitroaniline to 2-aminoaniline take place within 750 seconds interval of time. During this time about 95% of the reactant is converted into product. The progress of reaction is shown in Fig. 13.

This is an example of the first-order reaction with a rate constant (k) is 0.2013 min^{-1}.

5.1.3 Nano-Ag catalyzed conversion of 3-Nitroaniline to 3-aminoaniline
Analytical grade 3-Nitroaniline ($C_6H_6N_2O_2$), Sodium Borohydride ($NaBH_4$), were procured from Sigma Aldrich. About 1mL ice-cold solution of 0.05 M $NaBH_4$ was taken in the quartz cuvette. Then, in the above solution about 1.5 mL 0.1mM 3-Nitroaniline solutions was drop-wise added. To this reaction mixture water suspension of 200 μL (0.1mg/ml) Ag nanoparticles were added. The absorption peaks responsible for -NO2 functional group is at wavelength 363 nm which decreases with progress of time. This indicates that complete conversion of 3-Nitroaniline to 3-aminoaniline take place within 780 seconds time interval. During this time about 75% of the reactant is converted into product. When we plot a graph of concentration verse time we get a straight line passing through origin. The progress of reaction is shown in Fig. 14.

This is an example of the first-order reaction with a rate constant (k) is 0.1005 min^{-1}.

5.1.4 Nano-Ag catalyzed conversion of 4-Nitroaniline to 4-aminoaniline

Analytical grade 4-Nitroaniline ($C_6H_6N_2O_2$), Sodium Borohydride ($NaBH_4$), were procured. About 1.5 ml ice-cold solution of 0.05 M $NaBH_4$ was taken in the quartz cuvette. Then, in the above solution about 0.5 mL 0.1mM 4-Nitroaniline solutions was drop-wise added. To this reaction mixture water suspension of 200 μL (0.1mg/ml) Ag nanoparticles were added. The absorption peak responsible for $-NO_2$ functional group is at wavelength 382 nm which decreases with progress of time whereas a new absorption at 280 nm makes its appearance which is responsible for $-NH_2$ group. This indicates that complete conversion of 4-Nitroaniline to 4-aminoaniline take place within 690 seconds time interval. During this time about 98% of the reactant is converted into product. The progress of reaction is shown in Fig. 15.

This is an example of the first-order reaction with a rate constant (k) is 0.2803 min^{-1}.

5.2 Nano-Ag catalyzed Dye Degradation:

Dye is an integral part which is used to impart color to materials. Textile industries heavily use nature and synthetic dye to color the fabric. The excess amount of dye is discharged which constitute major sources of water pollution. A dye is a high molecular weight organic compound. Such type of high molecular weight compounds is not easily degraded through natural process. Thus it contaminates surface water reservoir, soil and environment for long period which affects aquatic flora and fauna. Therefore, attempts have been made by researchers to degrade high molecular weight organic compounds into simple molecules. Herein Ag nanoparticles act as nano-catalyst for the degradation reactions of methylene blue and crystal violet using UV light. These two dyes methylene blue and crystal violet are selected for our study because they shows different colours in the oxidized and reduced forms and also their absorption maximum does not overlap with the SPR band of AgNPs[28,37-39].

5.2.1 Nano-Ag catalyzed degradation of Methylene blue (MB)

Methylene blue solution was prepared by dissolving 10 ppm of methylene blue (Methylthioninium Chloride) ($C_{16}H_{18}ClN_3S$) in 80 mL of double-distilled water. In the methylene blue solution 100 mg synthesized Ag nanoparticles were added which behaves as heterogeneous catalyst. Then the beaker is wrapped with aluminum foil so as to avoid exposure of light. The solution in the beaker was rotated with magnetic needle. This results in adsorption of dye stuff on surface of nanoparticles. The reaction system was kept in darkness for two hours. Then after two hours reaction system was kept in light and absorption was measured at definite interval of time. The spectrophometric analysis was carried out both under ultraviolet light and visible light so as to investigate the efficiency of nanoparticles.

The photocatalytic efficacy of AgNPs was determined both in UV radiation and visible light. Methylene blue was used as a test contaminant since it has been extensively used as an indicator for the photocatalytic activities owing to its absorption peaks in the visible range. The Uv-vis analysis reveals that about 80% degradation of dye takes place in 180 minutes. This is an example of first order kinetic reaction with rate constant 0.00985 min^{-1}. The phocatalytic degradation of dye is spectrophotometrically monitored and shown in Fig. 16.

5.2.2 Nano-Ag catalyzed degradation of Crystal violet (CV):

Crystal violet or gentian violet is a triaryl methane dye. In fact crystal violet is not only a dye but is a multi-applicative compound which finds use in bacterial staining, used as anti-bacterial, antifungal and antihelmentic medicine especially used as poultry medicine by veterinary doctors. When dissolved in water dye imparts blue-violet shade. Crystal violet solution was prepared by dissolving 10 ppm of crystal violet (Tris(4-(dimethylamino)phenyl) methylium chloride)($C_{25}H_{30}N_3Cl$) in 80 mL double distilled water. Then 100mg Ag nanoparticle was dispersed. The beaker was completely wrapped with aluminum foil and kept on magnetic stirrer and rotated. The beaker was kept in darkness for two hours. The evaluation was carried out both under ultraviolet radiation and visible light so as to investigate the efficiency of nanoparticles. The Uv-vis analysis reveals that about 75% degradation of dye takes place in 120 minutes. This is an example of first order kinetic reaction with rate constant 0.0281 min^{-1}. The phocatalytic degradation of dye is spectrophotometrically monitored and shown in Fig. 17.

6. Conclusion

Herein we have successfully synthesized Ag nanoparticles using Indian cow (A-2) urine. As cow urine is used as reducing agent this method of synthesis is very much cost effective and environmentally benign. In fact, Ag nanoparticles are synthesized from the waste product alone. Bio-synthesized Ag nano-particles are potent catalyst for organic transformation reactions. The progress of organic transformation was monitored using spectrophotomer. The synthesized nanoparticle could successfully degrade organic dyes such as methylene blue and crystal violet.

Declarations

Conflict of Interest

There is no conflict of interest for the publication of article.

References

(1)   Types of Metal and Their Applications | Classification of Metals https://fractory.com/types-of-metal/ (accessed Jun 27, 2020).

(2)   Mixture | CK-12 Foundation https://flexbooks.ck12.org/cbook/ck-12-chemistry-flexbook-2.0/section/2.7/primary/lesson/mixtures-ms-ps (accessed Jun 27, 2020).

(3)   Capek, I. Chapter 1 Nanotechnology and Nanomaterials. In *Nanocomposite Structures and Dispersions: Science and Nanotechnology : Fundamental Principles and Colloidal Particles (Studies in Interface Science Book 23)*; 2006; Vol. 23, pp 1–69. https://doi.org/10.1016/s1383-7303(06)80002-5.

(4)   ASHBY, M. F. *MATERIALS SELECTION IN IN MECHANICAL DES*, 1992; Vol. 3. https://doi.org/10.1017/CBO9781107415324.004.

(5)   Prasad, S. R.; Padvi, M. N.; Shaikh, Y. I.; Suryawanshi, S. S.; Samant, A. P; Chaudhary, L. S.; Prasad, N. R. Bio - Inspired Synthesis of Catalytically and Biologically Active Palladium Nanoparticles Using Bos Taurus Urine. *SN Appl. Sci.* **2020**, No. February. https://doi.org/10.1007/s42452-020-2382-3.

(6)   Gavade, N. L.; Kadam, A. N.; Suwarnkar, M. B.; Ghodake, V. P; Garadkar, K. M. Biogenic Synthesis of Multi-Applicative Silver Nanoparticles by Using Ziziphus. *Spectrochim. ACTA PART A Mol. Biomol. Spectrosc.* **2014**, *136*, 953–960. https://doi.org/10.1016/j.saa.2014.09.118.

(7)   Hankare, P. P.; Sanadi, K. R.; Garadkar, K. M.; Delekar, S. D.; Mulla, I. S. Effect of Cobalt Doping on Structural and Thermoelectrical Power of Zinc Allu Chromites Synthesised by Sol – Gel Auto-Combustion Method. *Mater. Lett.* **2013**, *110*, 42–44. https://doi.org/10.1016/j.matlet.2013.07.087.

(8)   Mubarakali, D.; Thajuddin, N.; Jeganathan, K.; Gunasekaran, M. Colloids and Surfaces B : Biointerfaces Plant Extract Mediated Synthesis of Silver and Gold Nanoparticles and Its Antibacterial Activity against Clinically Isolated Pathogens. *Colloids Surfaces B Biointerfaces* **2011**, *85* (2), 360–365. https://doi.org/10.1016/j.colsurfb.2011.03.009.

(9)   Santoshi, A. Green Synthesis , Characterization and Catalytic Activity of Palladium Nanoparticles by Xanthan Gum. **2015**, *5*, 315–320. https://doi.org/10.1007/s13204-014-0320-7.

(10)   Amornkitbamrung, L.; Pienpinijtham, P.; Thammacharoen, C.; Ekgasit, S. Spectrochimica Acta Part A : Molecular and Biomolecular Spectroscopy Palladium Nanoparticles Synthesized by Reducing Species Generated during a Successive Acidic / Alkaline Treatment of Sucrose. *Spectrochim. Acta Part A Mol. Biomol. Spectrosc.* **2014**, *122*, 186–192. https://doi.org/10.1016/j.saa.2013.10.095.

(11)   Brand-Williams, W.; Cuvelier, M. E.; Berset, C. Use of a Free Radical Method to Evaluate Antioxidant Activity. *LWT Food Sci. Technol.* **1995**, *30*, 25–30. https://doi.org/. https://doi.org/10.1016/S0023-6438(95)80008-5.

(12)   Thakkar, K. N.; Mhatre, S. S.; Parikh, R. Y. Biological Synthesis of Metallic Nanoparticles. *Nanomedicine Nanotechnology, Biol. Med.* **2009**, *6* (March 2019), 257–262.

https://doi.org/10.1016/j.nano.2009.07.002.

(13) Korake, P. V; Dhabbe, R. S.; Kadam, A. N.; Gaikwad, Y. B.; Garadkar, K. M. Highly Active Lanthanum Doped ZnO Nanorods for Photodegradation of Metasystox. *J. Photochem. Photobiol. B Biol.* **2013**, *130*, 11−19. https://doi.org/10.1016/j.jphotobiol.2013.10.012.

(14) Prabhu, S.; Poulose, E. K. Silver Nanoparticles : Mechanism of Antimicrobial Action , Synthesis , Medical Applications , and Toxicity Effects. **2012**, *2*, 1−10.

(15) Rogoff, R. BLOOD SUGAR LEVEL SENSING AND MONITORING TRANSDUCER, 1985.

(16) Dongale, T. D.; Mohite, S. V.; Bagade, A. A.; Gaikwad, P. K.; Patil, P. S.; Kamat, R. K.; Rajpure, K. Y. Development of Ag/WO3/ITO Thin Film Memristor Using Spray Pyrolysis Method. *Electron. Mater. Lett.* **2015**, *11* (6), 944−948. https://doi.org/10.1007/s13391-015-4180-4.

(17) Monticone, F.; Alù, A. Metamaterials and Plasmonics: From Nanoparticles to Nanoantenna Arrays, Metasurfaces, and Metamaterials. *Chinese Phys. B* **2014**, *23* (4). https://doi.org/10.1088/1674-1056/23/4/047809.

(18) Remita, H.; Saha, A.; Sharma, G. K. Investigation into the Catalytic Activity of Porous Platinum Nanostructures. *Langmuir* **2013**, *29*, 11431−11439. https://doi.org/10.1021/la401302p.

(19) Minocheherhomji, F. P.; Vyas, B. M. Study of the Antimicrobial Activity of Cow Urine and Medicinal Plant Extracts on Pathogenic Human Microbial Strains. *Int. J. Adv. PHARMACY, Biol. Chem.* **2014**, *3* (4), 836−840.

(20) Kora, A. J.; Rastogi, L. Green Synthesis of Palladium Nanoparticles Using Gum Ghatti (Anogeissus Latifolia) and Its Application as an Antioxidant and Catalyst. *Arab. J. Chem.* **2018**, *11* (7), 1097−1106. https://doi.org/10.1016/j.arabjc.2015.06.024.

(21) Sathishkumar, M.; Sneha, K.; Kwak, I. S.; Mao, J.; Tripathy, S. J.; Yun, Y. S. Phyto-Crystallization of Palladium through Reduction Process Using Cinnamom Zeylanicum Bark Extract. *J. Hazard. Mater.* **2009**, *171* (1−3), 400−404. https://doi.org/10.1016/j.jhazmat.2009.06.014.

(22) Deka, P.; Deka, R. C.; Bharali, P. In Situ Generated Copper Nanoparticle Catalyzed Reduction of 4-Nitrophenol. *New J. Chem.* **2014**, *38* (4), 1789−1793. https://doi.org/10.1039/c3nj01589k.

(23) Minocheherhomji, F. P. A Study of Antimicrobial Effect of Cow Urine on Pathogenic Human Microbial Strains , and the Comparative Study of the Combined Effect of Cow Urine with Medicinal Herbs , to Evaluate Their Potential ., SHRI JAGDISHPRASAD JHABARMAL TIBREWALA UNIVERSITY, VIDYANAGARI, JHUNJHUNU, RAJASTHAN − 333001, 213AD.

(24) Sahiner, N.; Karakoyun, N.; Alpaslan, D.; Aktas, N. Biochar-Embedded Soft Hydrogel and Their Use in Ag Nanoparticle Preparation and Reduction of 4-Nitro Phenol. *Int. J. Polym. Mater. Polym. Biomater.* **2013**,

62 (11), 590–595. https://doi.org/10.1080/00914037.2013.769163.

(25)   Aditya, T.; Jana, J.; Singh, N. K.; Pal, A.; Pal, T. Remarkable Facet Selective Reduction of 4-Nitrophenol by Morphologically Tailored (111) Faceted Cu2O Nanocatalyst. *ACS Omega* **2017**, *2* (5), 1968–1984. https://doi.org/10.1021/acsomega.6b00447.

(26)   Divband, B.; Khatamian, M.; Eslamian, G. R. K.; Darbandi, M. Synthesis of Ag/ZnO Nanostructures by Different Methods and Investigation of Their Photocatalytic Efficiency for 4-Nitrophenol Degradation. *Appl. Surf. Sci.* **2013**, *284*, 80–86. https://doi.org/10.1016/j.apsusc.2013.07.015.

(27)   Moraes, L. E.; Burgos, S. A.; DePeters, E. J.; Zhang, R.; Fadel, J. G. Short Communication: Urea Hydrolysis in Dairy Cattle Manure under Different Temperature, Urea, and PH Conditions. *J. Dairy Sci.* **2017**, *100* (3), 2388–2394. https://doi.org/10.3168/jds.2016-11927.

(28)   Suryavanshi, R. D.; Mohite, S. V.; Shaikh, S. K.; Thorat, J. B.; Rajpure, K. Y. Spray Deposited Fe2O3 Photoelectrode for Degradation of Benzoic Acid and Methyl Blue Dye under Solar Radiation. *J. Mater. Sci. Mater. Electron.* **2018**, *29* (24), 20875–20884. https://doi.org/10.1007/s10854-018-0230-7.

(29)   Vinila, V. S.; Jacob, R.; Mony, A.; Nair, H. G.; Issac, S.; Rajan, S.; Nair, A. S.; Isac, J. XRD Studies on Nano Crystalline Ceramic Superconductor PbSrCaCuO at Different Treating Temperatures. *Cryst. Struct. Theory Appl.* **2014**, *03* (01), 1–9. https://doi.org/10.4236/csta.2014.31001.

(30)   Theivasanthi, T.; Alagar, M. Titanium Dioxide (TiO2) Nanoparticles XRD Analyses: An Insight. **2013**. https://doi.org/(http://arxiv.org/abs/1307.1091).

(31)   Bakhtiari-Sardari, A.; Mashreghi, M.; Eshghi, H.; Behnam-Rasouli, F.; Lashani, E.; Shahnavaz, B. Comparative Evaluation of Silver Nanoparticles Biosynthesis by Two Cold-Tolerant Streptomyces Strains and Their Biological Activities. *Biotechnol. Lett.* **2020**, *42* (10), 1985–1999. https://doi.org/10.1007/s10529-020-02921-1.

(32)   Vijayan, R.; Joseph, S.; Mathew, B. Green Synthesis of Silver Nanoparticles Using Nervalia Zeylanica Leaf Extract and Evaluation of Their Antioxidant, Catalytic, and Antimicrobial Potentials. *Part. Sci. Technol.* **2019**, *37* (7), 805–815. https://doi.org/10.1080/02726351.2018.1450312.

(33)   Parang, Z.; Keshavarz, A.; Farahi, S.; Elahi, S. M.; Ghoranneviss, M.; Parhoodeh, S. Sharif University of Technology Fluorescence Emission Spectra of Silver and Silver / Cobalt Nanoparticles. *Sci. Iran.* **2012**, *19* (3), 943–947. https://doi.org/10.1016/j.scient.2012.02.026.

(34)   Liu, C.; Yang, X.; Yuan, H.; Zhou, Z.; Xiao, D. Preparation of Silver Nanoparticle and Its Application to the Determination of Ct -DNA. *sensors* **2007**, *7*, 708–718. https://doi.org/https://doi.org/10.3390/s7050708.

(35)   Sang, S.; Li, D.; Zhang, H.; Sun, Y.; Jian, A.; Zhang, Q.; Zhang, W. Facile Synthesis of AgNPs on Reduced Graphene Oxide for Highly Sensitive Simultaneous Detection of Heavy Metal Ions. *RSC Adv.* **2017**,

7 (35), 21618–21624. https://doi.org/10.1039/c7ra02267k.

(36)   Baruah, B.; Gabriel, G. J.; Akbashev, M. J.; Booher, M. E. Facile Synthesis of Silver Nanoparticles Stabilized by Cationic Polynorbornenes and Their Catalytic Activity in 4-Nitrophenol Reduction. *Langmuir* **2013**, *29* (13), 4225–4234. https://doi.org/10.1021/la305068p.

(37)   Joseph, S.; Mathew, B. Microwave-Assisted Green Synthesis of Silver Nanoparticles and the Study on Catalytic Activity in the Degradation of Dyes. *J. Mol. Liq.* **2015**, *204*, 184–191. https://doi.org/10.1016/j.molliq.2015.01.027.

(38)   Desai, M. P.; Sangaokar, G. M.; Pawar, K. D. Kokum Fruit Mediated Biogenic Gold Nanoparticles with Photoluminescent, Photocatalytic and Antioxidant Activities. *Process Biochem.* **2018**, *70* (March), 188–197. https://doi.org/10.1016/j.procbio.2018.03.027.

(39)   Liu, Y.; Hou, C.; Jiao, T.; Song, J.; Zhang, X.; Xing, R.; Zhou, J.; Zhang, L.; Peng, Q. Self-Assembled AgNP-Containing Nanocomposites Constructed by Electrospinning as Efficient Dye Photocatalyst Materials for Wastewater Treatment. *Nanomaterials* **2018**, *8* (1). https://doi.org/10.3390/nano8010035.
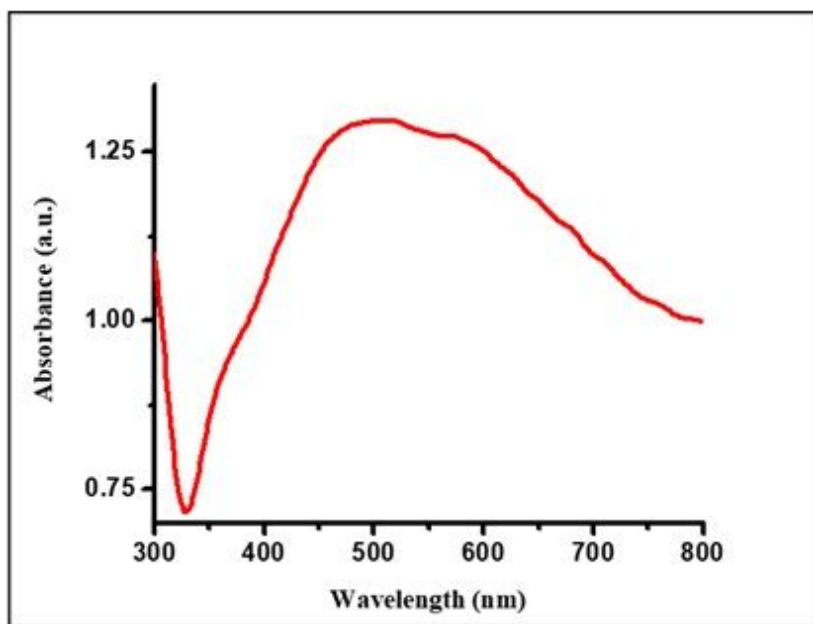
Figures

Figure 1

UV-Vis spectrum of Ag Nanoparticle
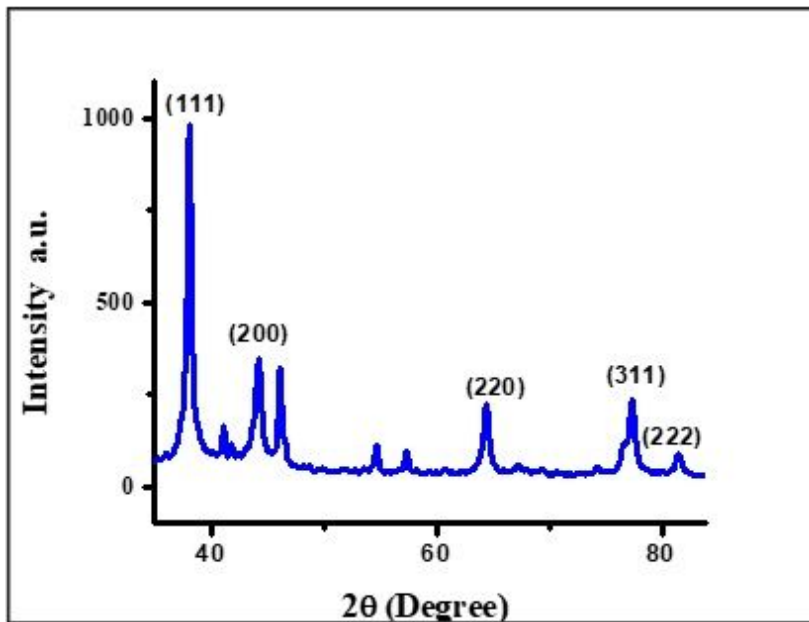
Figure 2

XRD Pattern of Ag Nanoparticle
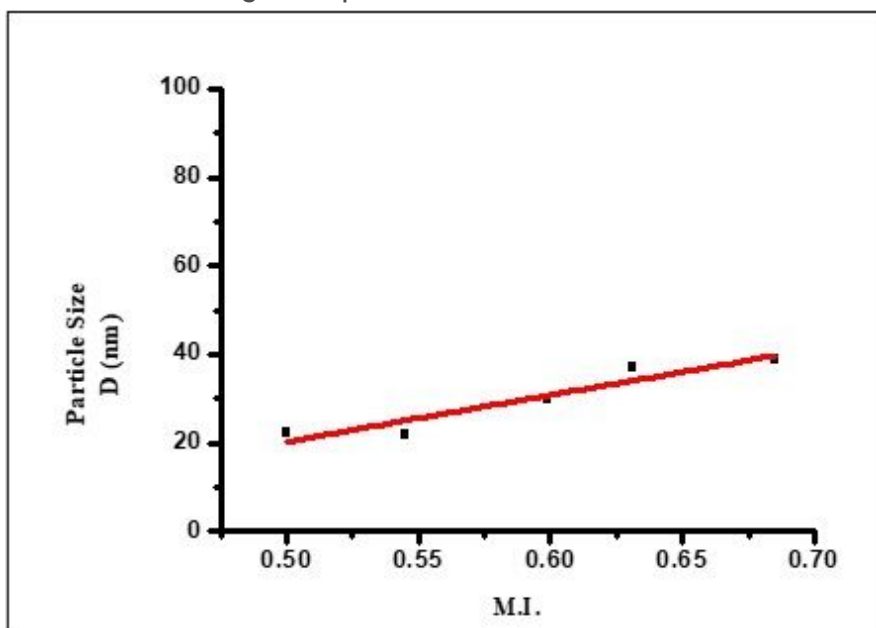
Figure 3

Morphological Index Vs Particle Size of Ag Nanoparticle
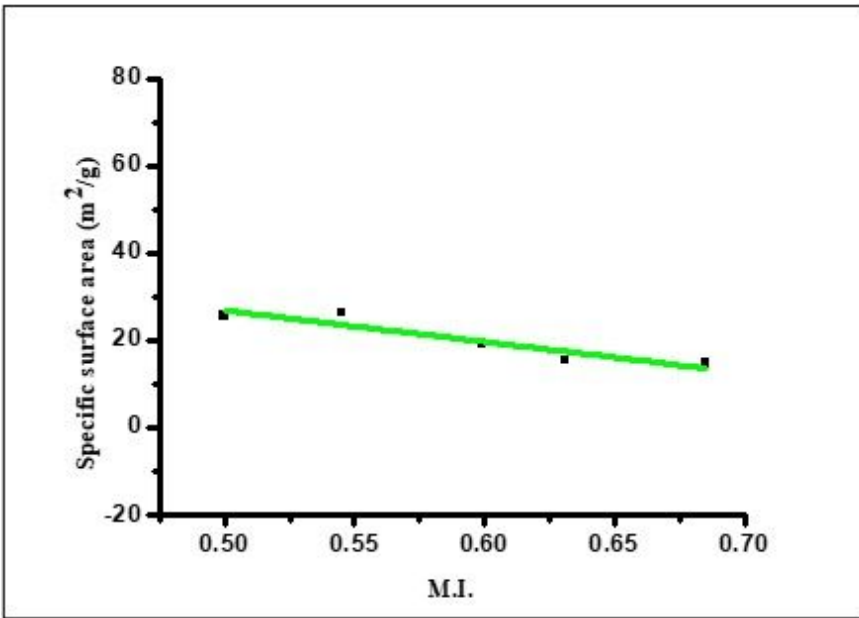
Figure 4

Morphological Index Vs Specific Surface Area of Ag Nanoparticle
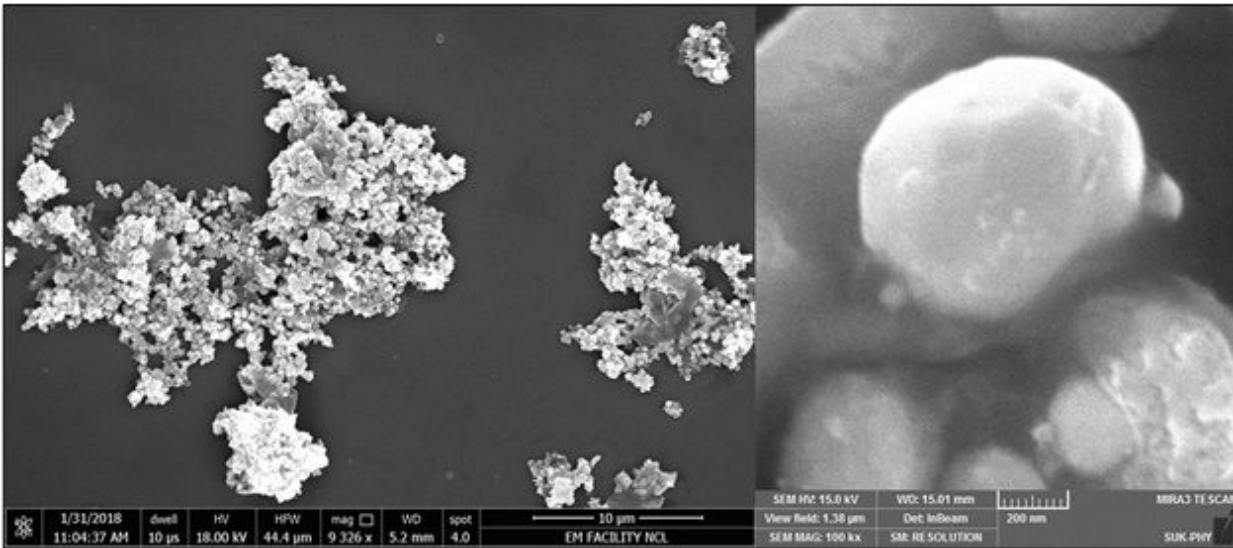
Figure 5

SEM Image of Ag Nanoparticle
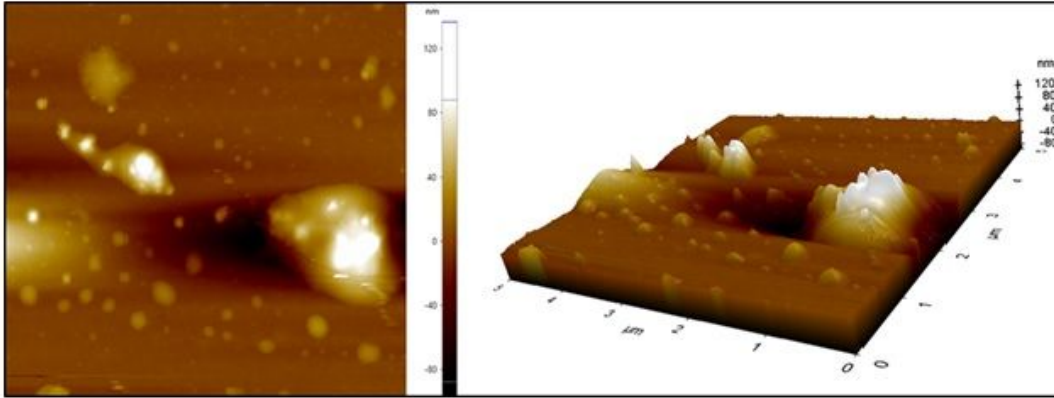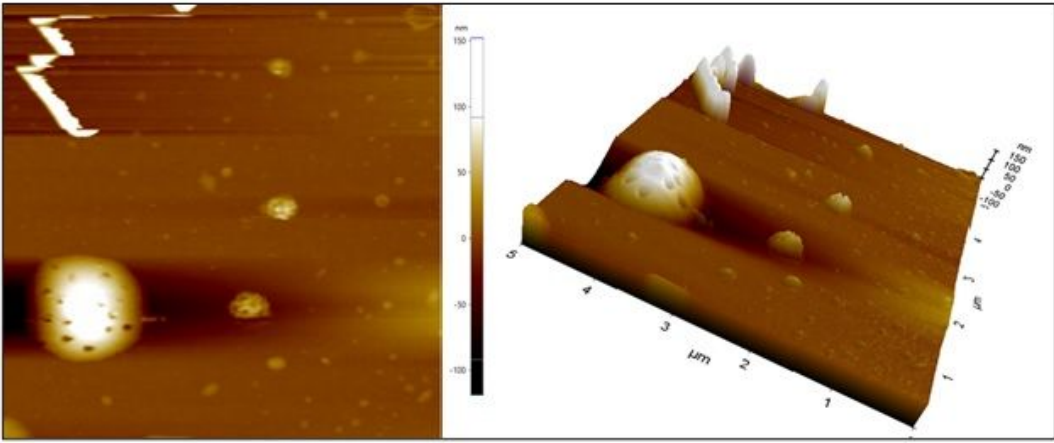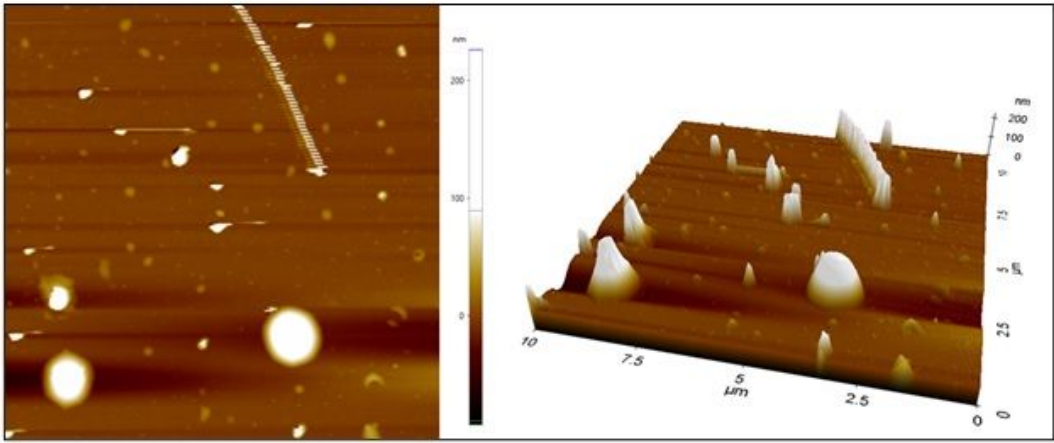
Figure 6

AFM 2D and 3D Images of Ag Nanoparticle
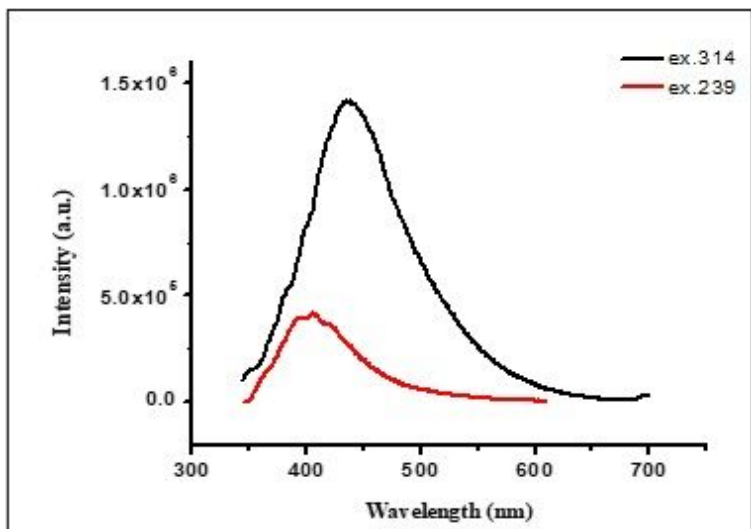
Figure 7

PL spectra of Ag Nanoparticle (excitation wavelength 239 & 314 nm)
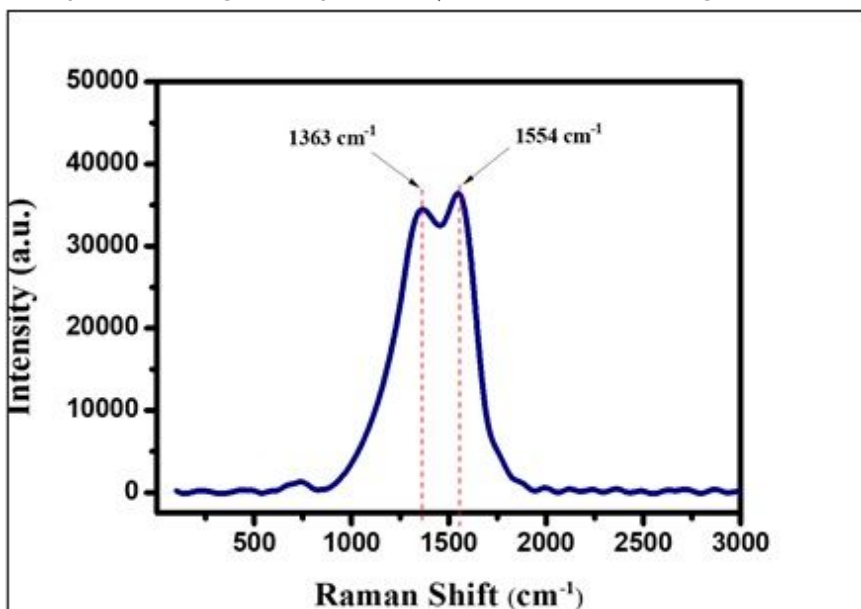
Figure 8

Raman spectrum of the Ag Nanoparticle
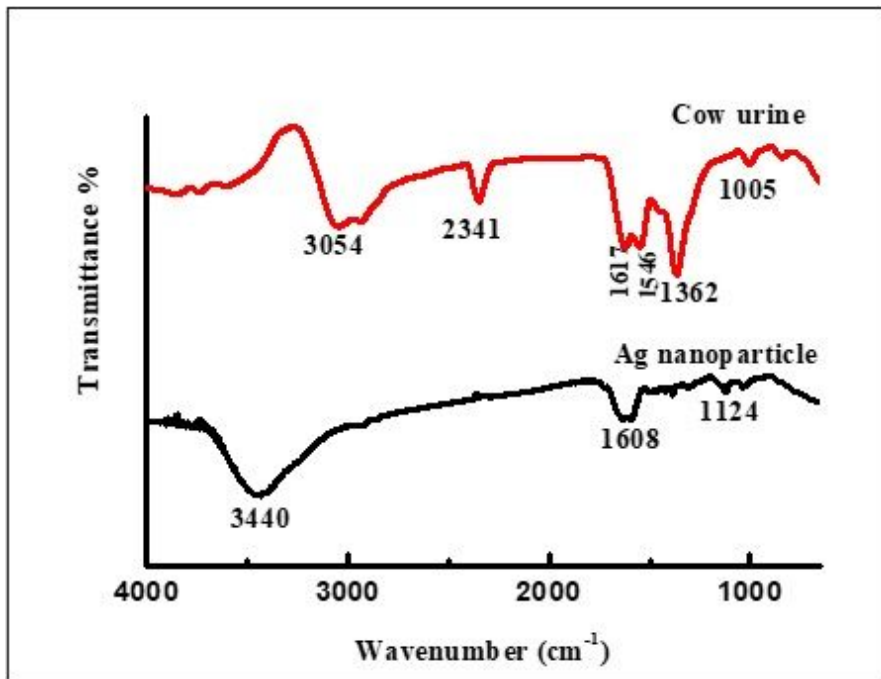
Figure 9

FT-IR spectra of the Ag Nanoparticle

Run	Mobility	Zeta Potential (mV)	Rel. Residual
1	-1.39	-17.82	0.0170
2	-1.61	-20.60	0.0225
3	-1.46	-18.65	0.0104
Mean	-1.49	-19.02	0.0166
Std. Error	0.06	0.82	0.0035
Combined	-1.48	-18.97	0.0132
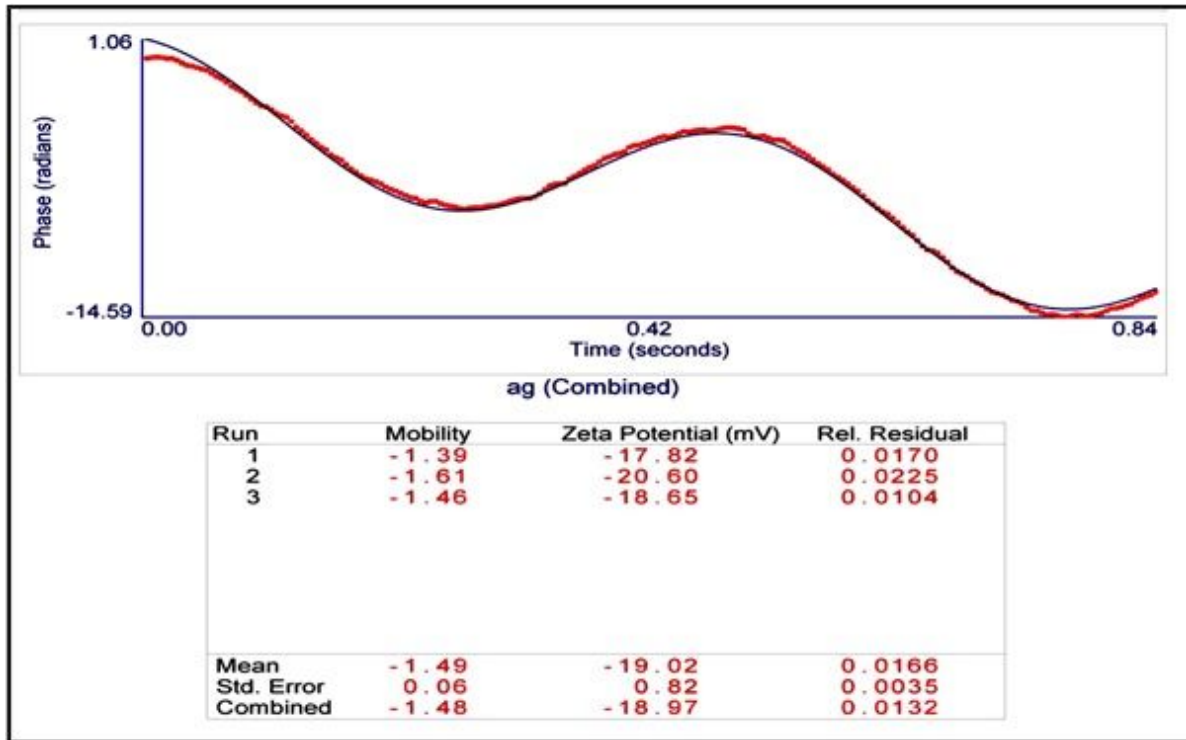
Figure 10

Zeta Potential of Ag Nanoparticle
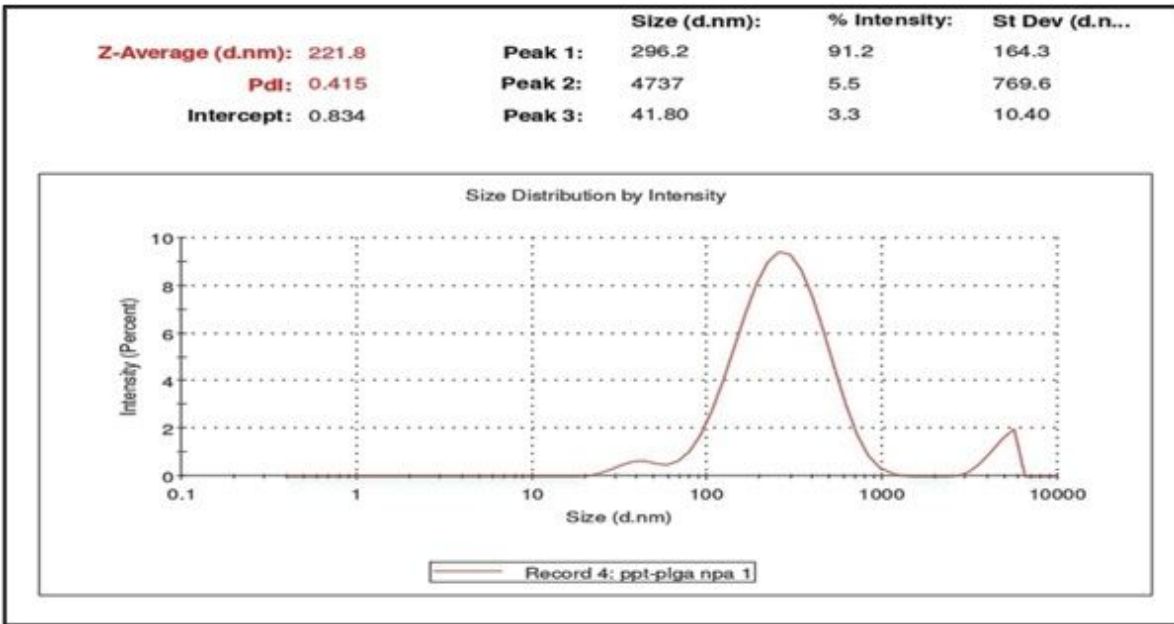
Figure 11

Dynamic Light Scattering of Ag Nanoparticle
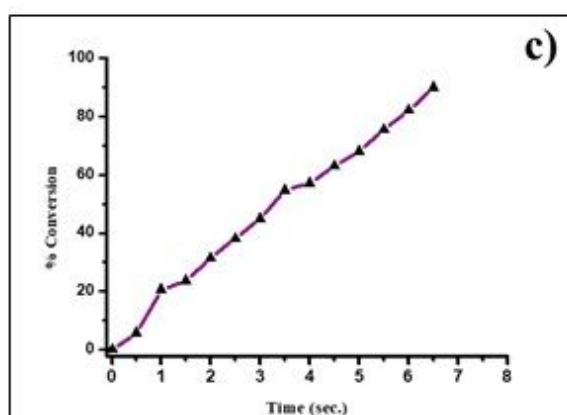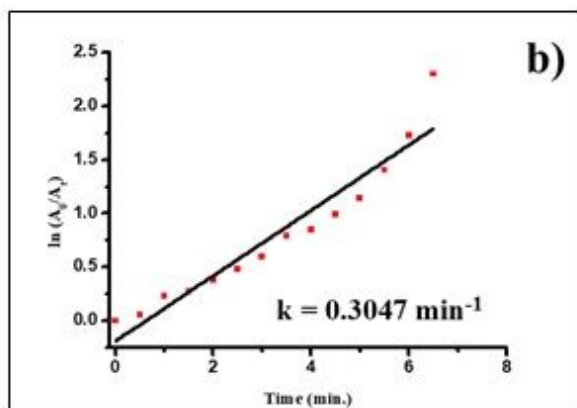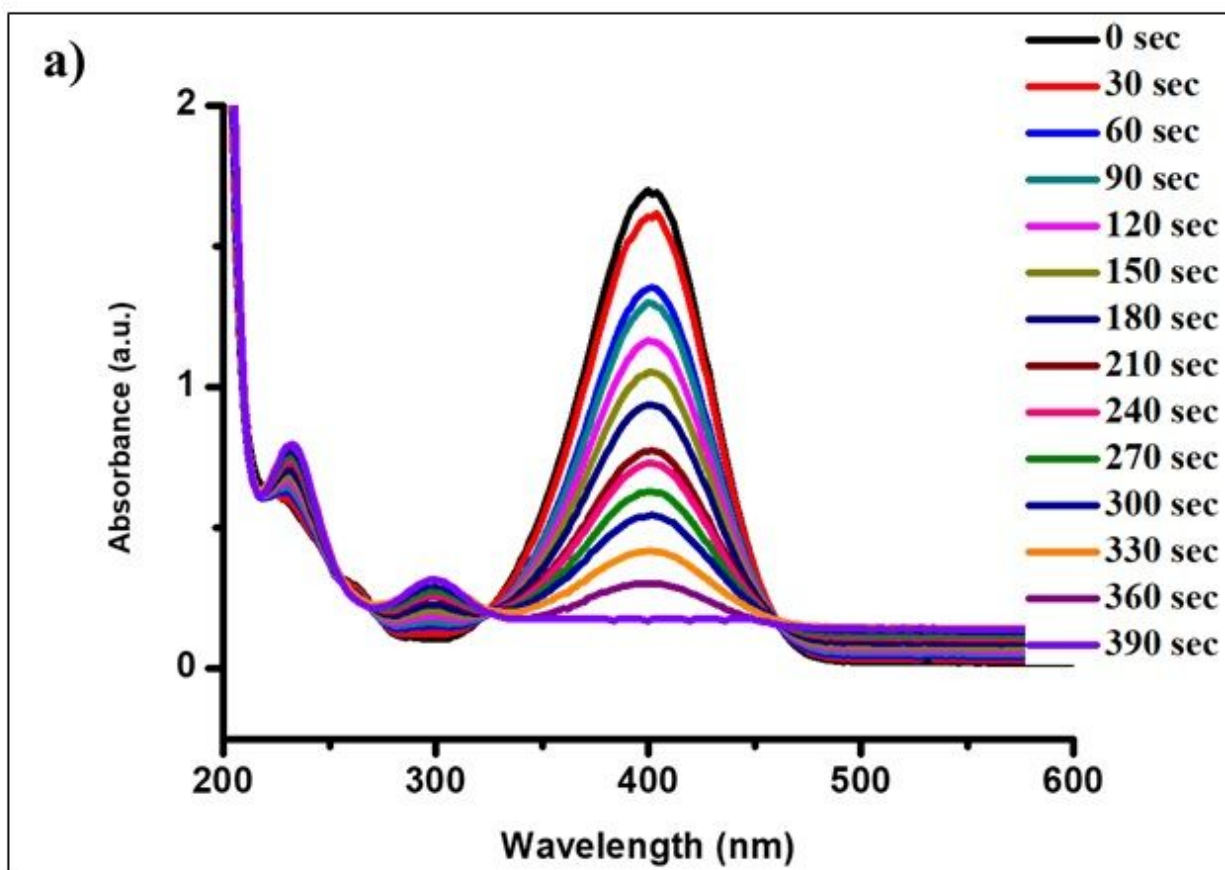
Figure 12

UV-Visible Spectra indicating (a) reduction of 4-Nitrophenol to 4- Aminophenol with time, (b) Kinetics of catalytic reduction and (c) Percentage conversion of 4-Nitrophenol
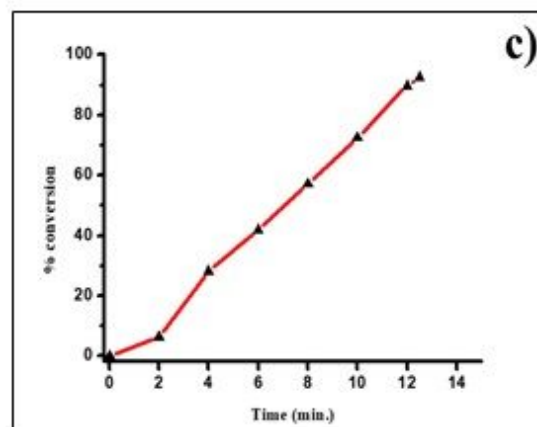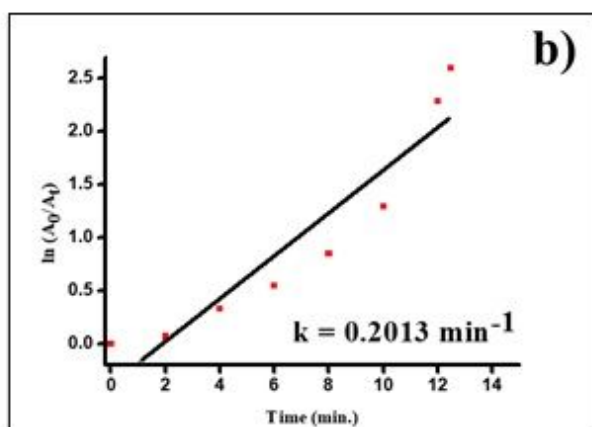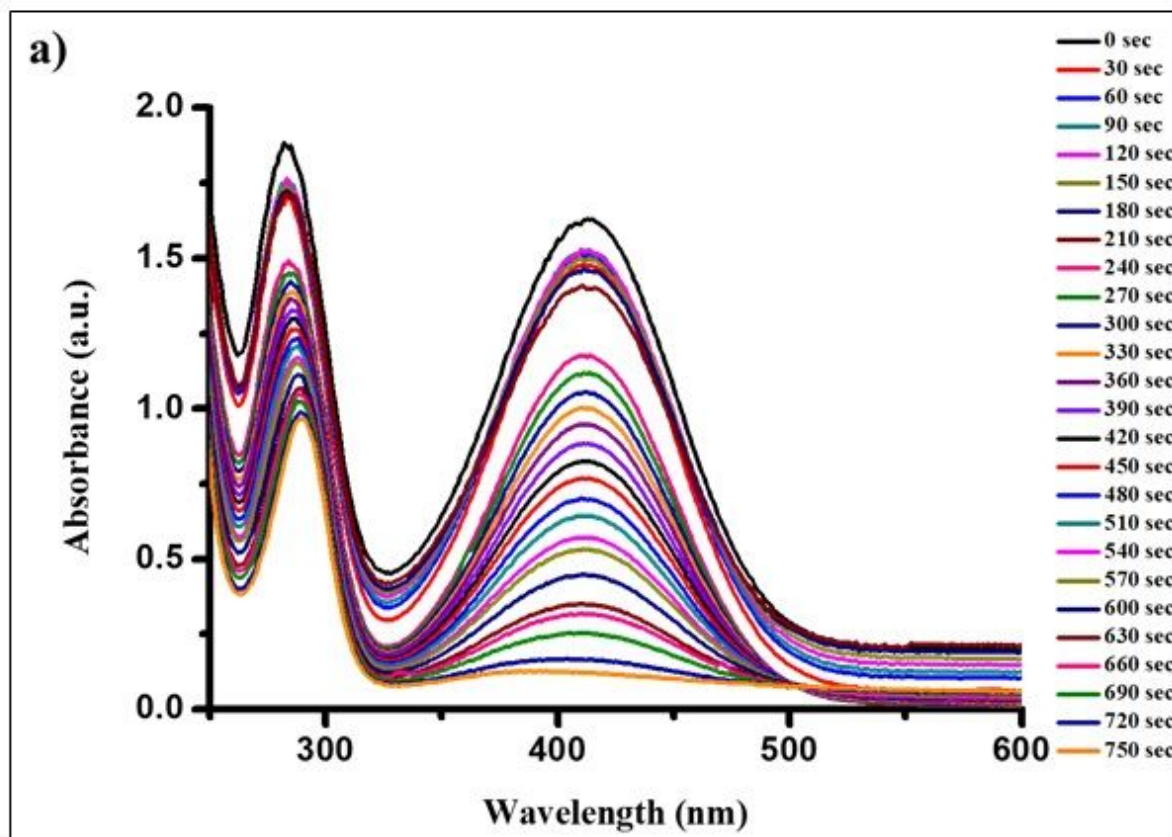
Figure 13

UV–vis absorption spectra of (a) 2-Nitroaniline, (b) Kinetics of catalytic reduction and (c) Percentage conversion of 2-Nitroaniline
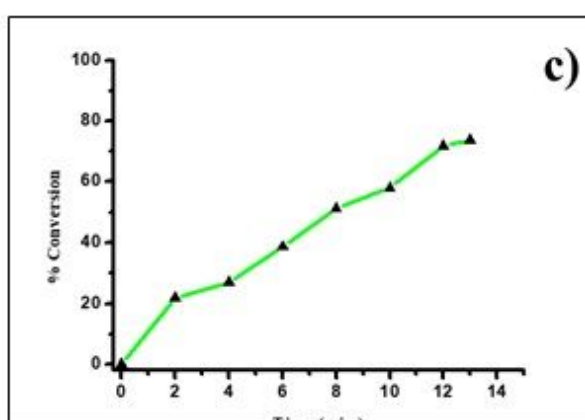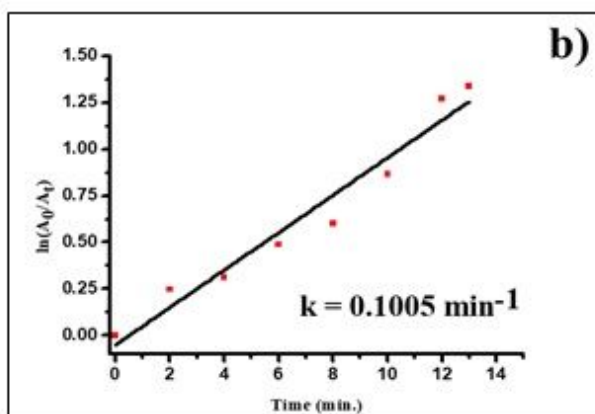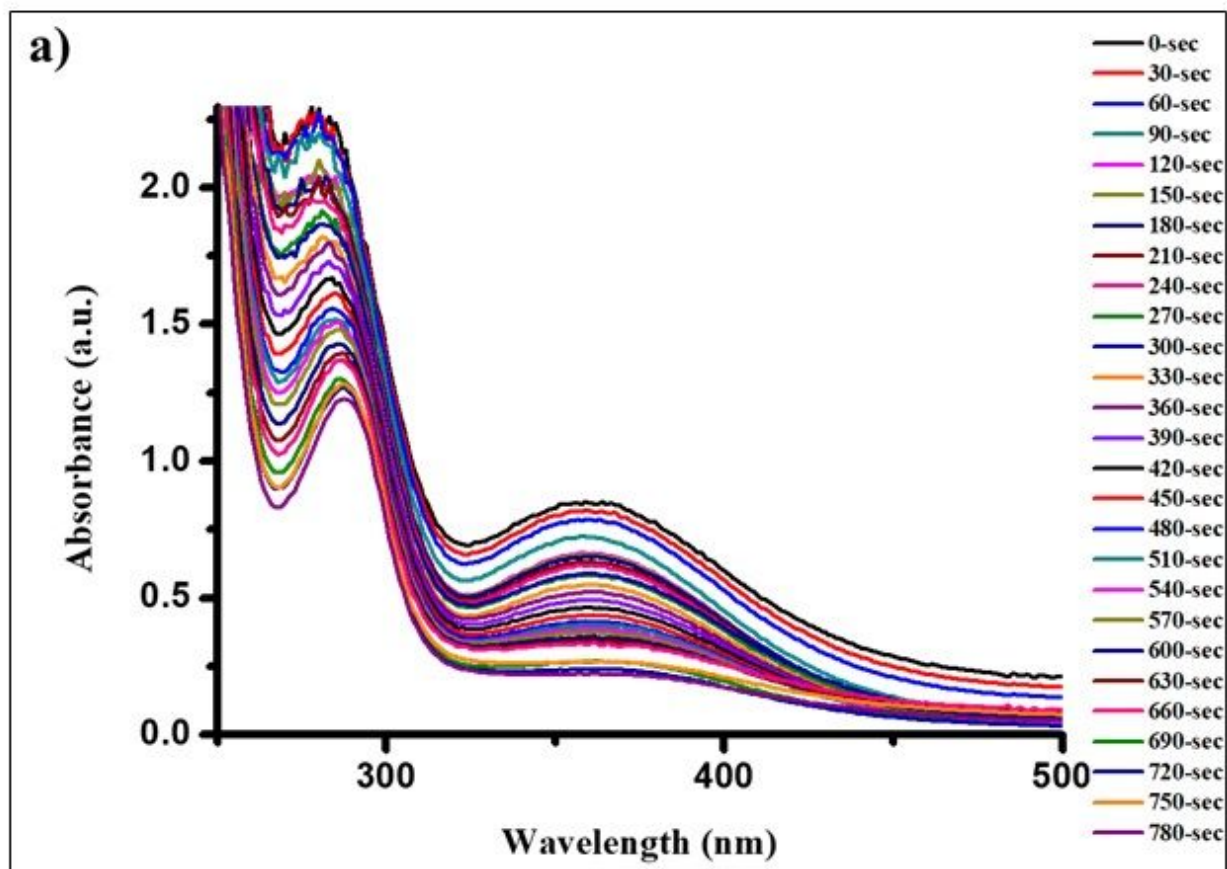
Figure 14

UV−vis absorption spectra of (a) 3-Nitroaniline, (b) Kinetics of catalytic reduction and (c) Percentage conversion of 3-Nitroaniline
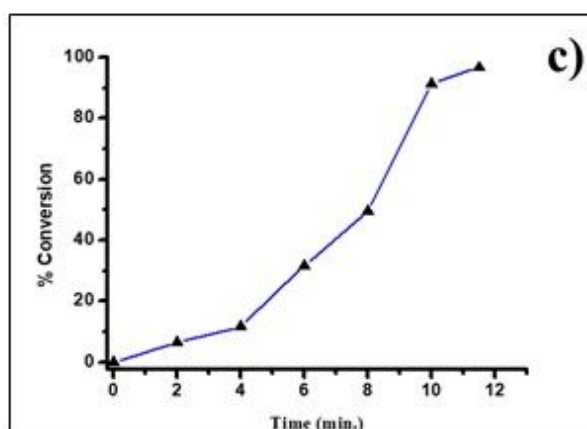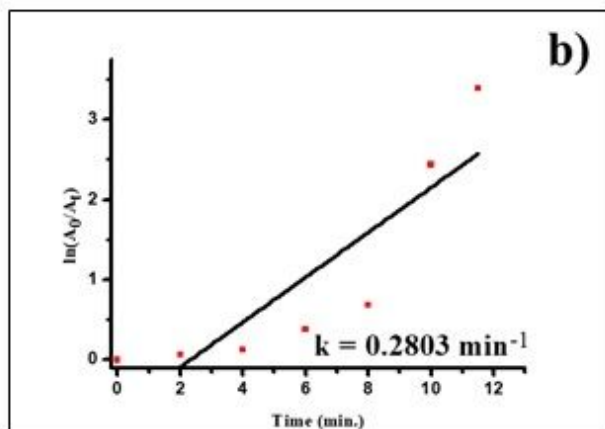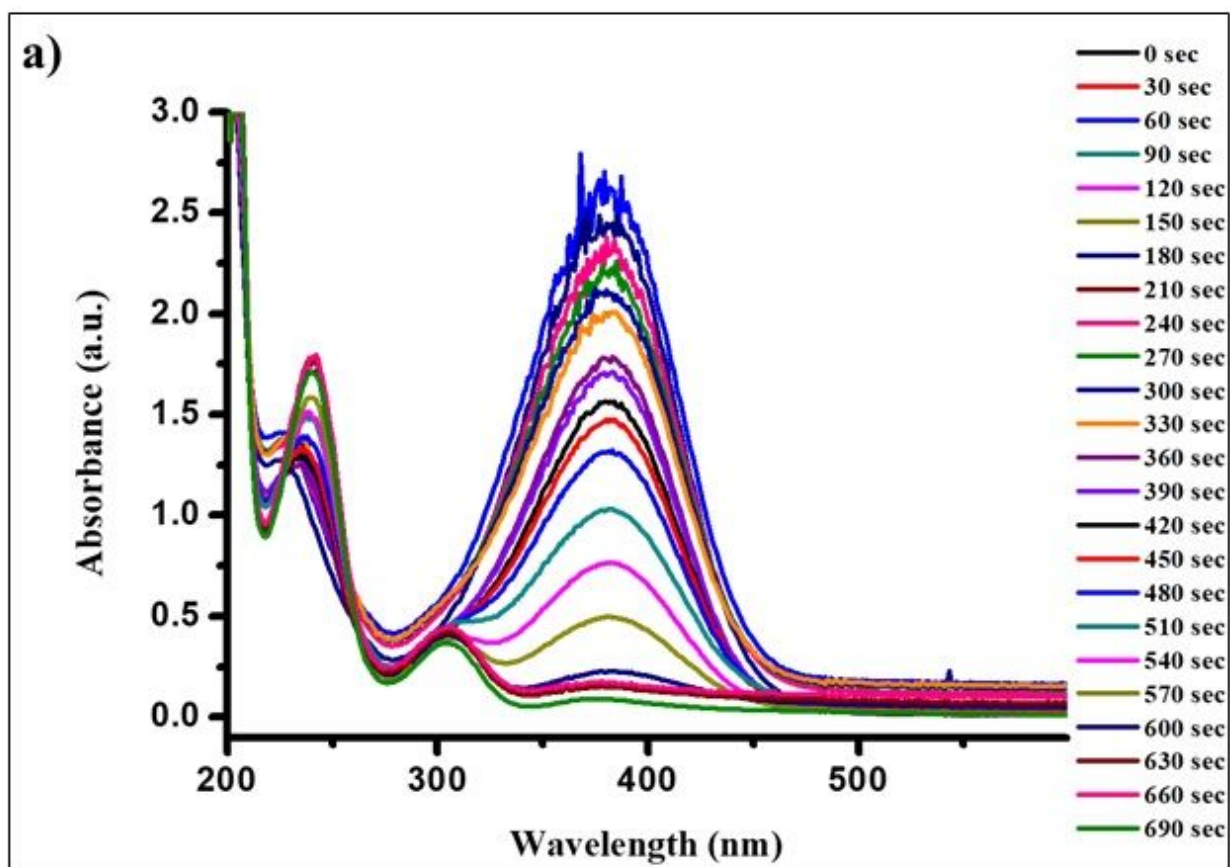
Figure 15

UV–vis absorption spectra of (a) 4-Nitroaniline, (b) Kinetics of catalytic reduction and (c) Percentage conversion of 4-Nitroaniline
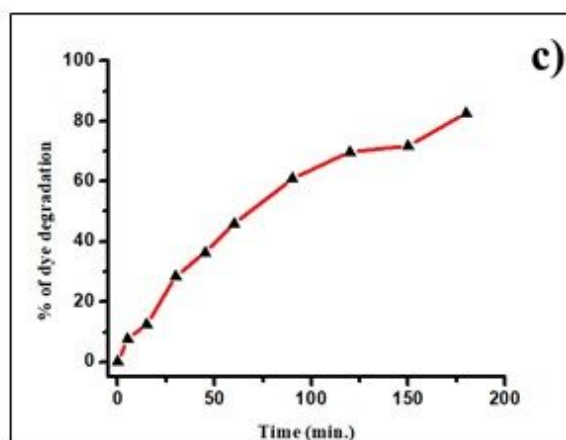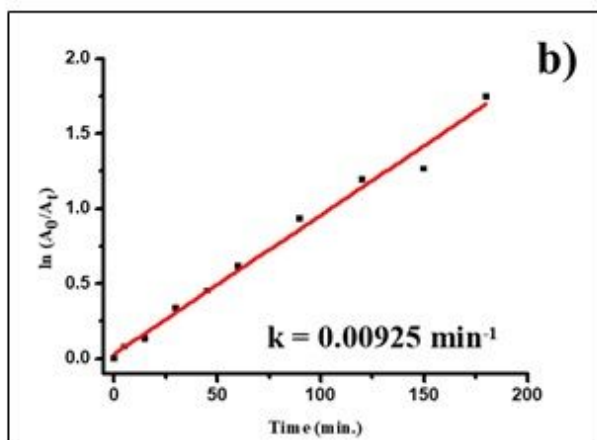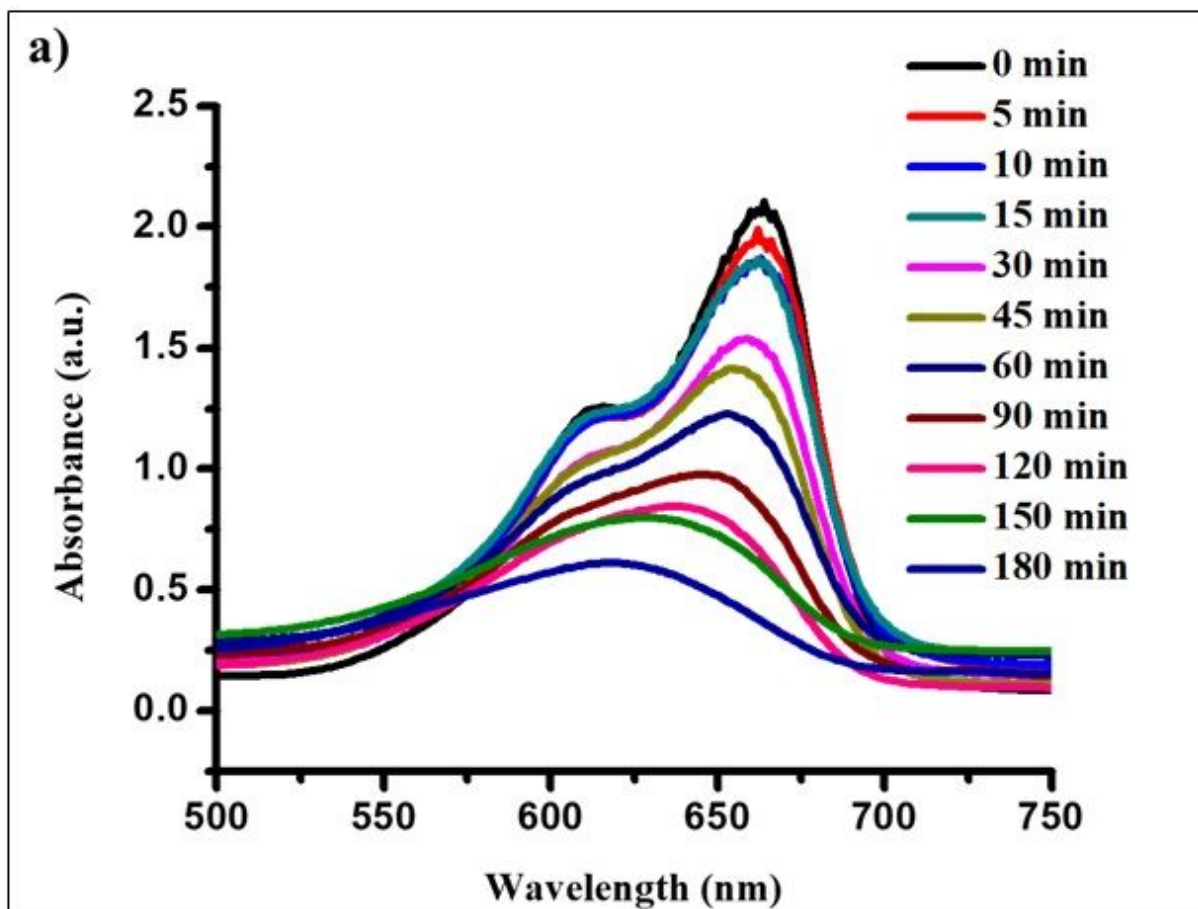
Figure 16

UV-vis absorption spectra of (a) Methylene Blue , (b)Kinetics of catalytic reduction and (c) Percentage Degradation of Methylene Blue
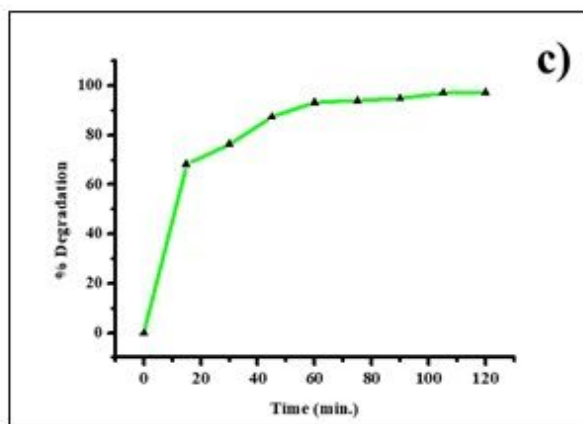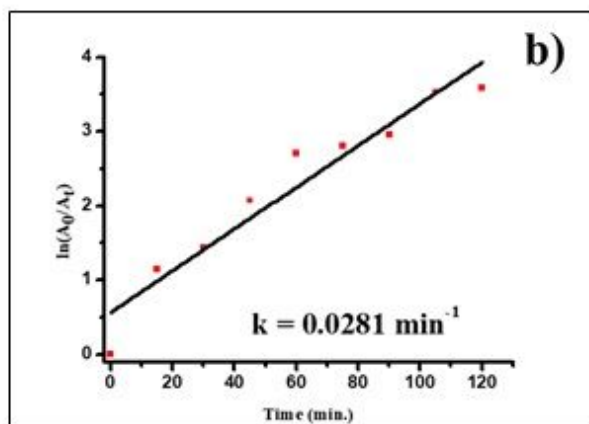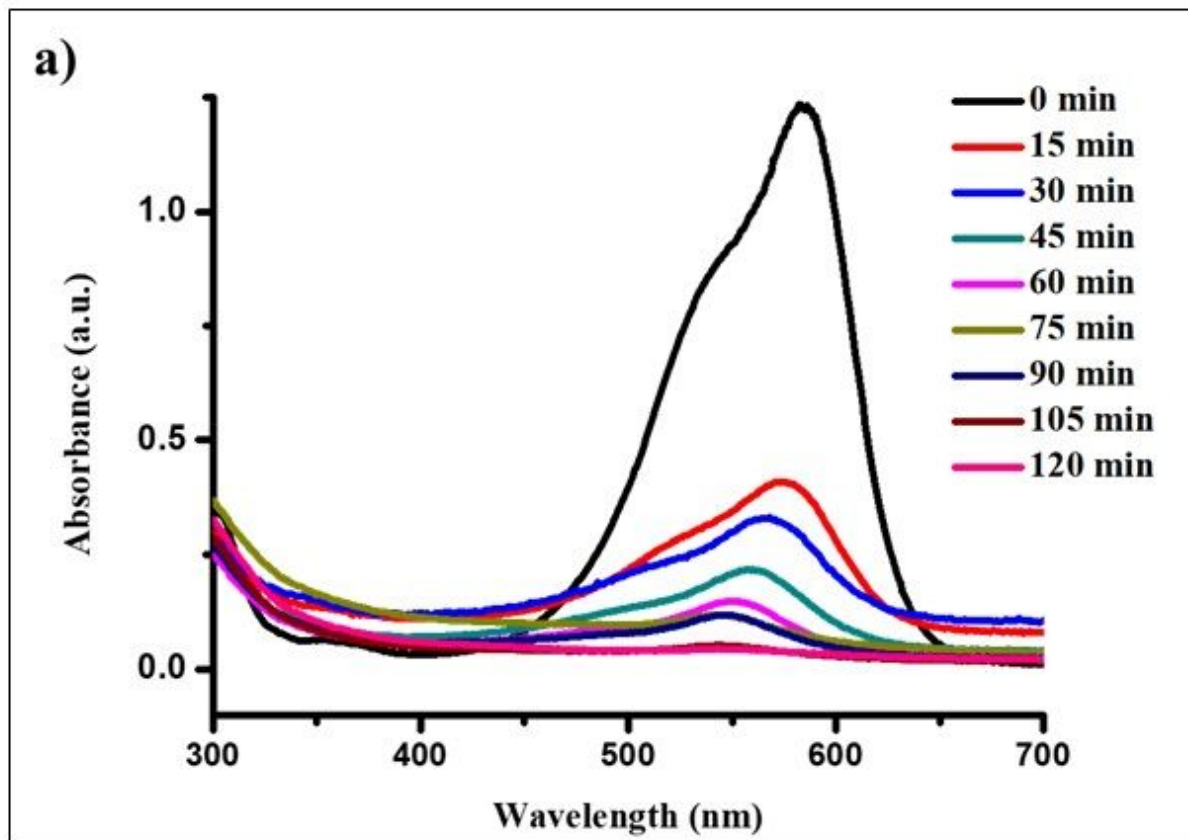
Figure 17

UV-vis absorption spectra of (a) Crystal Violet, (b)Kinetics of catalytic reduction and (c) Percentage Degradation of Crystal Violet